

TiO_2/SnO_2 electron transport double layers with ultrathin SnO_2 for efficient planar perovskite solar cells

Can Li(李灿), Hongyu Xu(徐宏宇), Chongyang Zhi(郅冲阳), Zhi Wan(万志), and Zhen Li(李祯)

Citation: Chin. Phys. B, 2022, 31 (**11**): 118802. DOI: 10.1088/1674-1056/ac8349

What follows is a list of articles you may be interested in

Reveal the large open-circuit voltage deficit of all-inorganicCsPbIBr$_2$ perovskite solar cells

Ying Hu(胡颖), Jiaping Wang(王家平), Peng Zhao(赵鹏), Zhenhua Lin(林珍华), Siyu Zhang(张思玉), Jie Su(苏杰), Miao Zhang(张苗), Jincheng Zhang(张进成), Jingjing Chang(常晶晶), and Yue Hao(郝跃)

Chin. Phys. B, 2022, 31 (**3**): 038804. DOI: 10.1088/1674-1056/ac464b

The effect of Mn-doped ZnSe passivation layer on the performance of CdS/CdSe quantum dot-sensitized solar cells

Yun-Long Deng(邓云龙), Zhi-Yuan Xu(徐知源), Kai Cai(蔡凯), Fei Ma(马飞), Juan Hou(侯娟), Shang-Long Peng(彭尚龙)

Chin. Phys. B, 2019, 28 (**9**): 098802. DOI: 10.1088/1674-1056/ab37f3

Nanoforest-like CdS/TiO_2 heterostructure composites: Synthesis and photoelectrochemical application

Shi Su(苏适), Jinwen Ma(马晋文), Wanlong Zuo(左万龙), Jun Wang(汪俊), Li Liu(刘莉), Shuang Feng(冯爽), Tie Liu(刘铁), Wuyou Fu(付乌有), Haibin Yang(杨海滨)

Chin. Phys. B, 2018, 27 (**8**): 088802. DOI: 10.1088/1674-1056/27/8/088802

TiO_2 composite electron transport layers for planar perovskite solar cells by mixed spray pyrolysis with precursor solution incorporating TiO_2 nanoparticles

Jiaqi Tian(田嘉琪), Hongcui Li(李红翠), Haiyue Wang(王海月), Bo Zheng(郑博), Yebin Xue(薛叶斌), Xizhe Liu(刘喜哲)

Chin. Phys. B, 2018, 27 (**1**): 018810. DOI: 10.1088/1674-1056/27/1/018810

420 nm thick $CH_3NH_3PbI_{3-x}Br_x$ capping layers for efficient TiO_2 nanorod array perovskite solar cells

Long Li(李龙), Cheng-Wu Shi(史成武), Xin-Lian Deng(邓新莲), Yan-Qing Wang(王艳青), Guan-Nan Xiao(肖冠南), Ling-Ling Ni(倪玲玲)

Chin. Phys. B, 2018, 27 (**1**): 018804. DOI: 10.1088/1674-1056/27/1/018804

SPECIAL TOPIC — Emerging photovoltaic materials and devices

TiO_2/SnO_2 electron transport double layers with ultrathin SnO_2 for efficient planar perovskite solar cells

Can Li(李灿), Hongyu Xu(徐宏宇), Chongyang Zhi(郅冲阳), Zhi Wan(万志), and Zhen Li(李祯)†

State Key Laboratory of Solidification Processing, Center for Nano Energy Materials, School of Materials Science and Engineering, Northwestern Polytechnical University, Xi'an 710072, *China*

(Received 12 June 2022; revised manuscript received 20 July 2022; accepted manuscript online 22 July 2022)

The electron transport layer (ETL) plays an important role on the performance and stability of perovskite solar cells (PSCs). Developing double ETL is a promising strategy to take the advantages of different ETL materials and avoid their drawbacks. Here, an ultrathin SnO_2 layer of ∼ 5 nm deposited by atomic layer deposit (ALD) was used to construct a TiO_2/SnO_2 double ETL, improving the power conversion efficiency (PCE) from 18.02% to 21.13%. The ultrathin SnO_2 layer enhances the electrical conductivity of the double layer ETLs and improves band alignment at the ETL/perovskite interface, promoting charge extraction and transfer. The ultrathin SnO_2 layer also passivates the ETL/perovskite interface, suppressing nonradiative recombination. The double ETL achieves outstanding stability compared with PSCs with TiO_2 only ETL. The PSCs with double ETL retains 85% of its initial PCE after 900 hours illumination. Our work demonstrates the prospects of using ultrathin metal oxide to construct double ETL for high-performance PSCs.

Keywords: atomic layer deposit, TiO_2, SnO_2, electron transport layer, stability

PACS: 88.40.hj, 81.15.Hi, 91.60.Ed, 72.20.Jv **DOI:** 10.1088/1674-1056/ac8349

1. Introduction

Perovskite solar cells (PSCs) have attracted great attention since their discovery in 2009.[1] It is considered an ideal candidate for the next-generation low-cost photovoltaics. The perovskite materials possess excellent optoelectronic properties, such as high absorption coefficient, defect tolerance, and tunable bandgap, which enables the rapid development of PSCs.[2–7] Currently, the record power conversion efficiency (PCE) of PSCs has reached 25.8%,[8] comparable to that of silicon solar cells. Further development focuses on improving the performance and stability of the PSCs to realize their commercial applications.

The PCE of PSCs depends on many factors, including the quality of the perovskite film,[9–13] defects at the perovskite interface,[14–18] and the properties of the carrier transport layers.[19–29] Especially, the electron transport layer (ETL) plays a vital role on the performance of the PSCs. Firstly, the surface property of the ETL directly influences the nucleation and growth process of the perovskite films. Secondly, the electrical properties of the ETL strongly influence the electron extraction and transport process. Thirdly, the defects at the ETL/perovskite interface and the chemical reactivity of the ETLs have profound impacts on the stability of PSCs.

TiO_2 as a conventional electron transport material in the dye sensitized solar cells, has been employed in PSCs from the early research.[30] TiO_2 with different crystallinity, morphology and fabrication methods have been intensively investigated in the PSCs.[31–34] However, the PSCs with TiO_2 ETLs showed severe instability issue as a consequence of the high chemical reactivity of TiO_2 under UV light. To address this issue, alternative metal oxide based ETLs are developed. SnO_2 is an attractive ETL in planar PSCs attributed to its higher carrier mobility, lower conduction band maximum (CBM) and smaller photooxidation tendency.[35–37] Developing TiO_2/SnO_2 double layer ETL combines the advantages of both TiO_2 and SnO_2. Kong and coworkers deposited an amorphous SnO_2 layer on top of TiO_2 by solution process for PSCs, and achieved a best PCE of 21.4%.[38] Gao *et al.* fabricated TiO_2/SnO_2 double ETL by spin-coating SnO_2 nanoparticles on the TiO_2 layer, yielding a PCE of 18.85%.[39] Few reports have investigated the influence of the thickness of SnO_2 layer in the double layer on the performance of the PSCs in a comprehensive way. Atomic layer deposit (ALD) approach is a sequential, self-limiting, and layer-by-layer process, which produces film with thickness of several nanometers without pinholes. It is highly suitable for understanding the influences of the compact and ultrathin SnO_2 layer in the double layer ETLs on the performance and stability of the PSCs.

Here, we developed an ultrathin SnO_2 layer to construct a TiO_2/SnO_2 double ETL for the planar PSCs. The ultrathin SnO_2 layers deposited by ALD process were 3–8 nm thick with outstanding compactness. With the TiO_2/ultrathin-SnO_2 double ETL, the PCE of the PSCs was significantly improved from 18.02% to 21.13%. The PCE of double ETL based PSCs highly depends on the thickness of the ultrathin SnO_2 layer. Additionally, the ultrathin SnO_2 layer protects the perovskite

†Corresponding author. E-mail: lizhen@nwpu.edu.cn

© 2022 Chinese Physical Society and IOP Publishing Ltd

from photocatalysis of TiO_2 layer. The PSCs with the double ETL retained 85% of its initial PCE after 900 hour continuous illumination. While the PCE of PSCs with TiO_2 only ETL quickly decayed to 64%. Our work demonstrates the prospect of employing ultrathin SnO_2 film to enhance the performance and stability of PSCs.

2. Methods

2.1. Materials

The 2,2′,7,7′-tetrakis-(N,N-di-4-methoxyphenylamino)-9,9′spirobifluorene) (Spiro-OMeTAD,99.9%), tris(2-(1H-pyrazol-1-yl)-4-tert-butylpyridine)-cobalt(III)tris(bis (trifluoromethylsulfonyl)imide) (FK209, 99%), bis(trifluoromethanesulfonyl)imide (Li-TFSI, 99%) and 4-tert-butyl pyridine (tBP, 96%) were purchased from Xi'an Polymer Light Technology Corp. Tetrakis(dimethylamido) tin (TMDASn) was purchased from KE-MICRO, Jiaxing. Formamidine iodide (FAI, 99.9%), methylammonium chlorine (MACl, 99.9%) and methylammonium bromine (MABr, 99.9%) were purchased from Great cell. Lead iodide (PbI_2, 99.9%) were purchased from TCI. Dimethylformamide (DMF, $>$ 99.9%), dimethyl sulfoxide (DMSO, 99.9%), chlorobenzene (CB, 99.9%) and acetonitrile were purchased from Sigma-Aldrich. All the reagents were used as received without any further purification.

2.2. Precursor solution preparation

The TiO_2 precursor solution (40 mmol/ml) was prepared by dissolving 900 μL $TiCl_4$ in 200 mL water. For the PbI_2 precursor solution, the PbI_2 powder was dissolved in the mixed solvent of DMF and DMSO (the volume ratio of 9:1) to form a solution of 1.5 M. For the FAI, MABr, and MACl precursor solution, FAI (90 mg), MABr (9 mg) and MACl (9 mg) was dissolved in 1 ml isopropanol. The hole transport layer (HTL) solution was prepared by dissolving 80 mg spiro-OMeTAD, 34 μL tBP, 24 μL Li-TFSI (520 mg/mL in acetonitrile) and 9 μL FK209 (320 mg/mL in acetonitrile) in 1 mL chlorobenzene.

2.3. Device fabrication

The FTO substrate was cleaned by surfactant, deionized water, acetone, isopropanol, and ethanol successively. After dried by the nitrogen gas, the FTO substrate was treated by UV-ozone for 15 min. To fabricate the TiO_2 layer by chemical bath deposit, the FTO substrate was immersed in the $TiCl_4$ aqueous solution (40 mmol/mL) and heated at 70 °C for 60 min. The FTO substrate was then rinsed with deionized water and ethanol sequentially, and then annealed at 200 °C for 30 min to obtain the TiO_2 compact layer.

The FTO/TiO_2 substrate was then transferred to the chamber of T-ALD 100A system to fabricate the ultrathin SnO_2 layer. The chamber was evacuated to a low pressure at 0.1 torr. TMDASn was used as the Sn source and heated at 55 °C and H_2O was employed as the O source. The deposit temperature was set to 160 °C. The deposit cycle was varied to tune the thickness of the SnO_2 layer. After the ALD process, the substrate was transferred to a nitrogen-filled glove box for the fabrication of the perovskite film.

The perovskite film was fabricated in a two-step approach. The PbI_2 precursor was first spun on to the double ETL layer at 2000 rpm for 30 s and then annealed at 70 °C for 1 min. The FAI, MAI, and MACl mixed solution was then spun on to the PbI_2 film at 2000 rpm for 30 s in the N_2-filled glovebox and then annealed at 150 °C for 15 min in the air to complete the perovskite conversion process. Afterwards, the HTL precursor solution was spun onto the perovskite film at 3000 rpm for 30 s in the glovebox. Finally, 80 nm Au electrodes were thermally evaporated in vacuum.

2.4. Measurement and characterization

The SEM images were recorded by FEI NAVA 450. The UV-vis absorption spectra were measured by UV-vis spectrophotometer (Lambda 35). PL spectra were measured using an Ocean Optics QE Pro spectrometer with an excitation wavelength of 532 nm. TRPL spectra were obtained using a Horiba PPD 900 spectrometer with an excitation wavelength of 405 nm. XPS measurements were performed using a Shimadzu Kratos photoelectron spectrometer. Simulated AM 1.5G sunlight was generated by a solar simulator (Newport, Sol3A). The light intensity (100 mW/cm^2) was calibrated by an ISO 17025-certified KG3-filterred silicon reference cell. The J–V characteristics of PSCs were recorded by a Keithley 2400 source-measurement The scan speed was 0.1 V/s ($-$0.1 V to 1.2 V). The incident photoelectron conversion efficiency (IPCE) was measured by a quantum efficiency measurement system (Enli Tech, QE-R3011). The cyclic voltammetry (CV) measurement was carried out in a three-electrode system with $Fe(CN)_6^{-3/-4}$ aqueous solution as the electrolyte and saturated calomel electrode as the reference electrode. The CV curves were recorded by CHI 760D electrochemical workstation. For the light stability measurement, the unencapsulated devices were stored in the nitrogen-filled glovebox and illuminated continuously under an LED light source. The illumination intensity of the LED was calibrated to introduce a J_{SC} in the PSCs equaling to the J_{SC} under simulated sunlight (100 mW/cm^2, AM 1.5G).

3. Results and discussion

Figure 1(a) shows the schematic diagram of the double ETL fabrication process. Briefly, a TiO_2 compact layer was first deposited on the fluorine-doped tin oxide (FTO) by chemical bath deposition (CBD). An ultrathin SnO_2 layer was then

deposited on TiO_2 using ALD process. The thickness of the SnO_2 was precisely controlled by the reaction cycles of the ALD process. Details of the TiO_2 and SnO_2 deposition are described in Section 2. Figure S1(a) shows the scanning electron microscopy (SEM) of TiO_2 layer on the FTO substrate. Since the TiO_2 layer has a thickness of only 25 nm measured from the profilometer, the FTO/TiO_2 retains the pristine morphology of the FTO substrate. The roughness of the substrate after TiO_2 deposition is 32.1 nm by atomic force microscopy (AFM) as shown in Fig. 1(b). The thickness of SnO_2 of one reaction cycle is calibrated by the profilometer (Fig. S2). The SnO_2 growth rate was approximately 0.0743 nm per ALD cycle. Therefore, the thickness of a typical SnO_2 layer with 70-cycle growth is around 5 nm. The ALD deposited SnO_2 layer exhibited outstanding conformality that the surface morphology of the ETL showed no obvious difference after SnO_2 deposition (Figs. S1(a) and S1(b)). The ALD SnO_2 layer filled the pinholes of the underlying TiO_2 layer. As a result, the surface roughness was slightly reduced to 31.2 nm after the SnO_2 deposition (Figs. 1(b) and 1(c)).

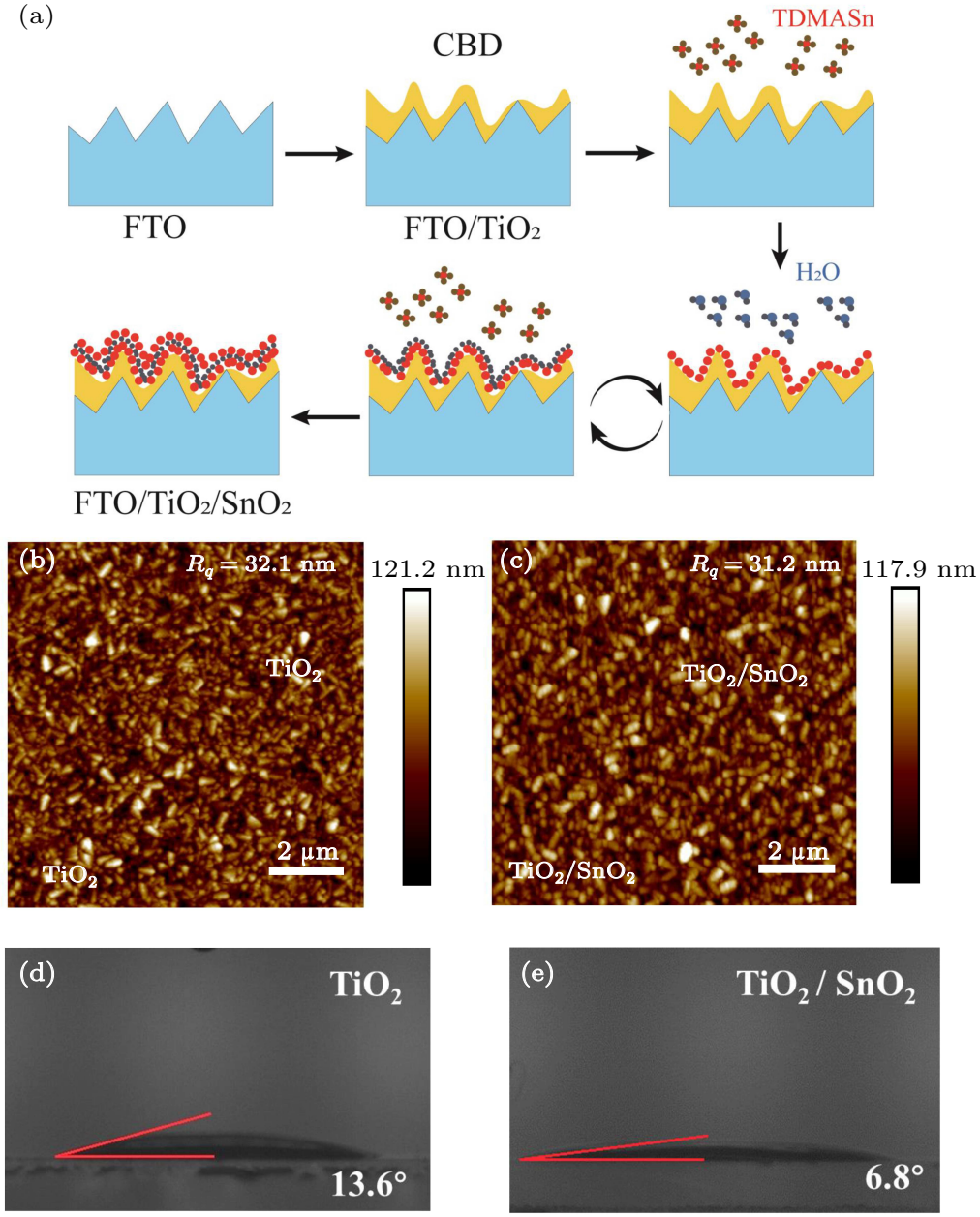


Fig. 1. (a) The schematic diagram of the TiO_2/SnO_2 double ETL fabrication process (tetrakis(dimethylamido) tin, TDMASn). The AFM images of (b) TiO_2 and (c) TiO_2/SnO_2. The water contact angle of (d) TiO_2 and (e) TiO_2/SnO_2 double ETL.

X-ray photoelectron spectroscopy (XPS) was performed to characterize the composition of the TiO_2/SnO_2 double ETL. Figure S3(a) demonstrates the full XPS spectrum of the double ETL. The full spectrum shows both strong Sn peaks and relatively weak Ti peaks. This indicates that the SnO_2 coating on the TiO_2 layer is thin enough to allow x-ray excited photoelectrons to penetrate through, given the penetration limit is only several nanometers. The Sn 3d spectrum is shown in

Fig. S3(b). The peaks at 486.4 eV and 494.8 eV correspond to the binding energies of Sn $3d_{5/2}$ and $3d_{3/2}$, representing the Sn(IV) valence state. The O peak at 529.5 eV (inset of Fig. S3(b)) comes from the Sn–O bonds.[40] XPS confirms that an ultrathin layer of SnO_2 is deposited on the surface of TiO_2.[41] To investigate the compactness of SnO_2 layer, cyclic voltammetry measurements were performed with bare FTO, FTO/TiO_2 and FTO/TiO_2/SnO_2 as the working electrode, respectively. $Fe(CN)_6^{3/4}$ aqueous solution was used as the electrolyte and saturated calomel electrode as the reference electrode. The results are compared in Fig. S4. For bare FTO, a strong redox peak is observed indicating fast and efficient redox reaction at the FTO/solution interface. When the FTO substrate is coated with TiO_2, the redox peak is suppressed due to the TiO_2 blockage effect. However, the redox peak is still resolvable because of the pinholes and leakage channel in the TiO_2. The redox reaction is further suppressed by the ultrathin SnO_2 coating, indicating that the ultrathin ALD SnO_2 layer is compact and fills the pinholes in the TiO_2 ETL.[42] Herein, a TiO_2/SnO_2 double ETL with an ultrathin but compact SnO_2 layer was successfully constructed using ALD process.

The ETL plays a significant role on the perovskite film quality because its morphology and wettability influence the nucleation and growth process of the perovskite crystals.[43] The wettability of the TiO_2 ETL was changed by the ultrathin SnO_2 layer coating. As shown in Figs. 1(d) and 1(e), the TiO_2 layer had a contact angle of 13.6°. The contact angle was reduced to 6.8° after SnO_2 deposition. The superior wettability of the double ETL facilitates the perovskite crystal growth to produce larger perovskite crystals and high-quality perovskite films. Figures S5(a) and S5(b) show the SEM images of the perovskite films deposited on the TiO_2-only ETL and TiO_2/SnO_2 double ETL, respectively. The perovskite film on TiO_2/SnO_2 double ETL showed a larger grain size. The average perovskite grain size increases from 550 nm on TiO_2 to 640 nm on the TiO_2/SnO_2 double ETL (Fig. S5(c)). The larger grain size would reduce grain boundary defects and enhance the optoelectronic properties of the perovskite films.

PSCs with the structure of FTO/ETL/perovskite/spiro-OMeTAD/Au were fabricated to investigate the effects of the ultrathin SnO_2 on the performance of PSCs. The schematic of the PSC structure is depicted in Fig. 2(a). The different functional layers are also labelled in the cross-sectional SEM images of PSCs in Fig. 2(b). As the thickness of the ultrathin SnO_2 layer is less than 10 nm, it cannot be differentiated in the cross-sectional SEM images. It can be seen that the perovskite crystals are compact and well aligned on the substrate and grow through the film without horizontal grain boundaries. The contact between the double ETL and perovskite layer is continuous without cracks or voids. The intimate contact promotes efficient electron extraction and transport in the PSCs.[44]

The photovoltaic performances of PSCs with the TiO_2 and TiO_2/SnO_2 ETLs are compared in Figs. 2(c) and 2(d). Figure 2(c) shows the *J*–*V* curves of the champion devices. The PSCs with TiO_2/SnO_2 double ETL exhibited an open-circuit voltage (V_{OC}) of 1.12 V, short-circuit current density (J_{SC}) of 24.49 mA·cm^{-2}, and fill factor (FF) of 78.34%, yielding a high PCE of 21.13%. In comparison, the PSC with TiO_2 ETL yielded a best PCE of 18.02%. The statistical distribution of photovoltaic parameters of PSCs with TiO_2 and TiO_2/SnO_2 ETLs are shown in Fig. S6. It can be seen that the V_{OC}, J_{SC} and FF were all improved by the double ETL. The corresponding incident photon-to-electron conversion efficiency (IPCE) spectra are shown in Fig. 2(d). The quantum efficiency of the PSC with double ETL is higher than that of the TiO_2 based PSCs in the whole perovskite absorption range, explaining the higher J_{SC} in the *J*–*V* curves.

As aforementioned, the thickness of the ultrathin SnO_2 layer can be precisely controlled by the deposit cycles, which is the advantages of ALD over other deposit techniques. The thickness of the ultrathin SnO_2 layer for the double ETL was optimized to achieve the best PSC performance. Figures 3(a) and S7 show the statistical distribution of photovoltaic parameters of the PSCs with different SnO_2 thicknesses. It is observed that the PSCs with 5 nm-thick SnO_2 exhibited the highest PCE. To elucidate the effects of the SnO_2 thickness on the final PCE of the PSCs, the optical and electrical properties of the ultrathin SnO_2 were studied. The transmittance spectra of the double ETL with different SnO_2 thickness are shown in Fig. 3(b). It is obvious that the transmittance of the double ETL is decreased when the SnO_2 thickness increases. Figure 3(c) shows the IPCE spectra of PSCs with different SnO_2 thickness. The IPCE results are consistent with the *J*–*V* curves, exhibiting the highest J_{SC} from the 5-nm thick SnO_2 based PSCs. When the SnO_2 thickness increases from 2 nm to 5 nm, the quantum efficiency in the range of 350 nm to 650 nm is increased. The higher quantum efficiency of 5 nm thickness SnO_2-based PSC in the short wavelength may be due to the reduced surface recombination at the perovskite/ETL interfaces. When the thickness is further increased to 8 nm, the quantum efficiency becomes lower in the full absorption range which could be due to the lower light transmittance of the 8 nm SnO_2.

The series and shunt resistances (R_s and R_{sh}) of PSCs with different ALD SnO_2 thickness are extracted from the *J*–*V* curves. As shown in Fig. 3(d), the R_s first decreases then increases slightly when the thickness of the ALD SnO_2 is increased from 0 to 8 nm, and the 5 nm SnO_2 device shows the lowest R_s. The R_{sh} increases with larger ALD SnO_2 thickness and plateaus at above 5 nm. The higher R_{sh} of the double ETL can suppress the undesired leakage current and improve the PCE. The thickness of the SnO_2 in the double ETL was fixed to 5 nm with the best PSC performance in the following investigation and discussion.

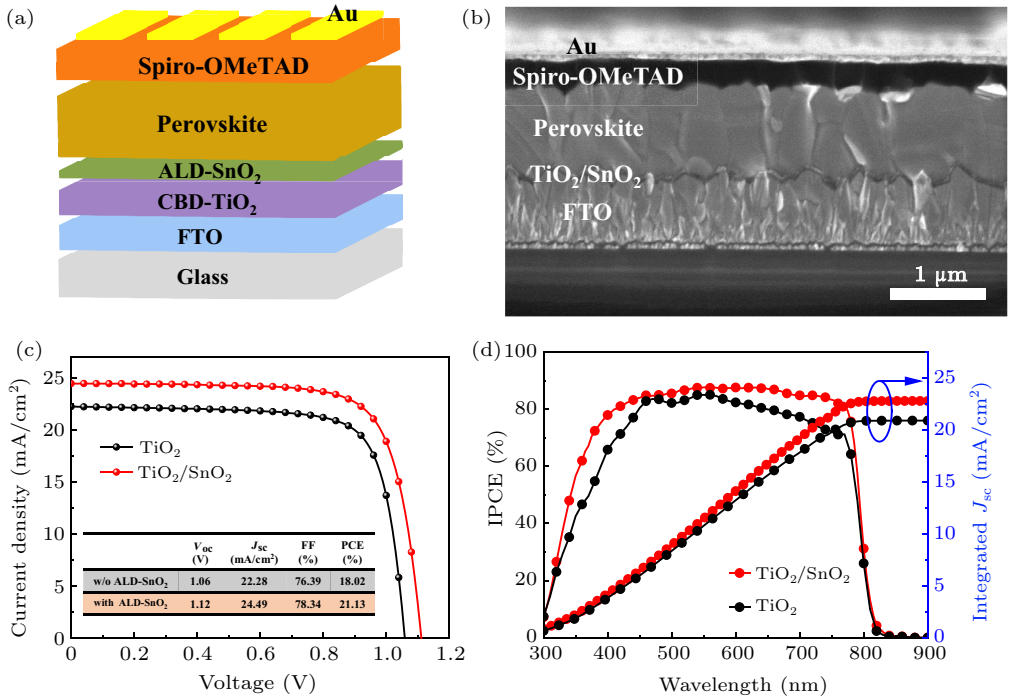


Fig. 2. Photovoltaic performance of the PSCs with double ETLs. (a) The schematic of the device structure and (b) the cross-sectional SEM images of the PSCs with TiO_2/SnO_2 double ETL. (c) The *J*–*V* curves of the champion devices with TiO_2 and TiO_2/SnO_2 based PSCs and (d) the corresponding IPCE spectra.

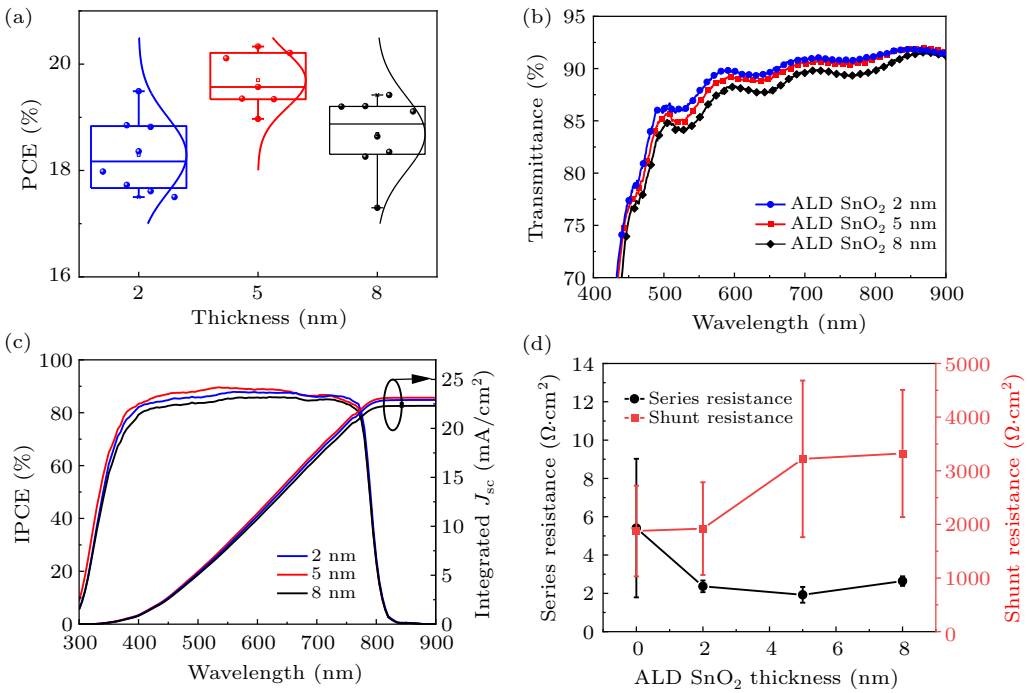


Fig. 3. (a) The PCE distribution of the TiO_2/SnO_2 double ETL based PSCs with different SnO_2 thicknesses; (b) the transmittance spectra of double ETL, (c) the IPCE spectra of PSCs, and (d) the series resistance and shunt resistance of the PSCs with the ultrathin SnO_2 at varied thickness.

To understand the mechanism of PCE improvement by the double ETL, we further investigated the optoelectronic properties of the double ETL. Figure S8(a) shows the transmittance spectra of the TiO_2 and TiO_2/SnO_2 ETLs. The transmittance was only slightly reduced between 400 nm and 450 nm due to the UV absorption of the SnO_2 layer. There was negligible absorption between 550 nm and 900 nm by the ultrathin SnO_2. On the other hand, the SnO_2 layer showed strong impact on the electrical conductivity as shown in Fig. S8(b). The structure of FTO/ETL/Ag was fabricated to measure the film conductivity. The electrical conductivity was improved from 2.49×10^{-4} S/cm of the single TiO_2 layer to 3.08×10^{-4} S/cm of the double ETL. The better conductivity of the double ETL may be due to the smooth surface that improves the interface contact and better energy level of the ETL to form an ohmic contact.

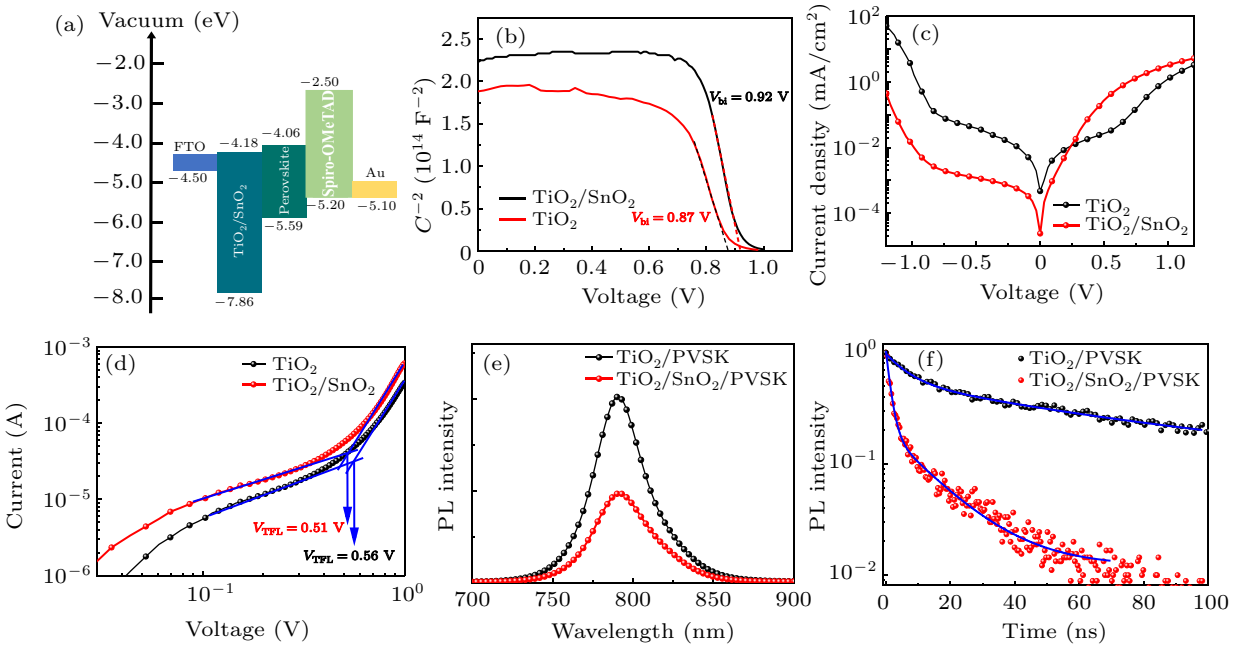


Fig. 4. Electrical and optoelectronic properties of the double ETLs: (a) the band structure of PSCs with the TiO_2/SnO_2 double ETL, (b) the Mott–Schottky analysis, (c) dark current density–voltage curves, and (d) space charge limited current (SCLC) characterization of perovskite films with TiO_2 and with TiO_2/SnO_2; (e) steady-state PL spectra and (f) time-resolved PL spectra of perovskite films on TiO_2 and TiO_2/SnO_2.

The absorption spectra of the perovskite films on TiO_2 and TiO_2/SnO_2 are similar (Fig. S9). The double ETL has little influence on the thickness and absorption of the perovskite films. Ultraviolet photoelectron spectroscopy (UPS) measurement was performed to characterize the band structure of the ETLs (Fig. S10(a)). The secondary electron cut-off energy was around 16.93 eV, corresponding to a work function of 4.29 eV. The valence band maximum (E_V) was −3.57 eV relative to the Fermi level. Therefore, the E_{VBM} of the TiO_2/SnO_2 double ETL was −7.86 eV relative to the vacuum level. The bandgap (E_g) of the SnO_2 was estimated to be 3.68 eV according to the Tauc plot (Fig. S10(b)). Thus, the conduction band minimum (E_C) was −4.18 eV following the equation

$$E_C = E_V + E_g. \tag{1}$$

The band diagram of the PSCs with double ETL is depicted in Fig. 4(a). The smaller conduction band energy offset between the double ETL and perovskite favors electron extraction from the perovskite films to the double ETL. The better band alignment between the double ETL and perovskite can improve the FF and J_{SC} of the PSCs in consistent to the J–V results. The built-in potential in the PSC was measured by Mott–Schottky to show the band alignment improvement by the double ETLs (Fig. 4(b)). The built-in potential (V_{bi}) is determined from the intercept of the linear portion of the Mott–Schottky[45] plot with the potential axis from the following equation:

$$\frac{1}{C^2} = \frac{-2}{Ne\epsilon\epsilon_0 A^2}(V - V_{bi}), \tag{2}$$

where C is the capacitance, N is the carrier density, ϵ_0 is the permittivity of free space, ϵ is the permittivity of the perovskite material, A is the area of the PSCs, e is the elementary charge, and V is the applied voltage. The built-in potential increased from 0.87 V with TiO_2-only ETL to 0.92 V with the double TiO_2/SnO_2 ETL. The higher built-in potential is due to the larger energy offset between the HTL and ETLs, which is beneficial for carrier separation in the PSCs. The increase of the built-in potential contributes to the V_{OC} improvement in the PSCs. The dark J–V curve of the PSCs was measured as shown in Fig. 4(c). It can be seen that the reverse saturation current was suppressed with the double ETL, owing to the reduced pin-holes in the ETL and better crystallinity of the perovskite film.

The space charge limited current (SCLC) measurements were conducted to characterize the defect density in the perovskite films.[46] The electron-only device was fabricated in the structure of FTO/double ETL (or TiO_2)/perovskite/PCBM/Au and the current–voltage curve is shown in Fig. 4(d). The defect density (N_{trap}) of the electrons in the perovskite film can be calculated using the equation

$$N_{trap} = \frac{2\epsilon\epsilon_0 V_{TFL}}{ed^2}, \tag{3}$$

where d is the thickness of the perovskite film, and V_{TFL} is the trap-filled limited voltage. The V_{TFL} of SCLC measurement for perovskite with TiO_2 and TiO_2/SnO_2 were 0.51 V and 0.56 V, respectively. Therefore, the defect density of the perovskite film decreased from 2.23×10^{15} cm^{-3} with TiO_2 to 2.03×10^{15} cm^{-3} with TiO_2/SnO_2. Consequently, the double ETL enhanced the perovskite film quality and reduced the defects density at the ETL/perovskite interface contributing to the suppressed nonradiative recombination and V_{OC} improve-

ment. The charge carrier dynamics was characterized by photoluminescence (PL). Figure 4(e) shows the steady-state PL of the perovskite films on TiO_2 and TiO_2/SnO_2. The perovskite PL intensity was reduced by the TiO_2/SnO_2 due to more efficient electron extraction. The carrier lifetime decreased from 108.1 ns with TiO_2 to 81.5 ns with TiO_2/SnO_2 fitted from the time-resolved PL spectra (Fig. 4(f)). The PL results suggest that the double ETL improves the electron extraction, matching with the better band alignment of the double ETLs. Overall, the TiO_2/SnO_2 double ETL reduces the interface defects, improves the band alignment of the ETL/perovskite interface and contributes to the higher PCE in the PSCs.

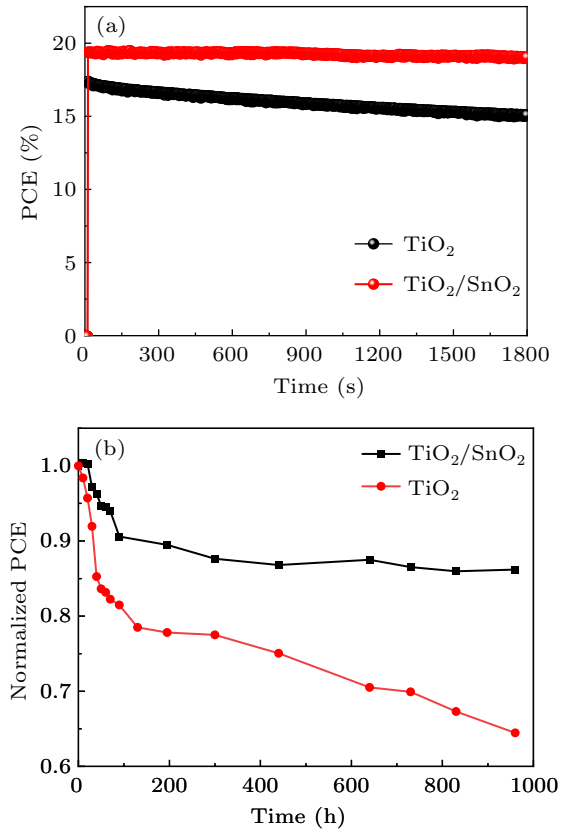


Fig. 5. (a) The stabilized power output measurements of PSCs with TiO_2 and TiO_2/SnO_2 double ETL; (b) the normalized PCE of PSCs with TiO_2 and TiO_2/SnO_2 under continuous illumination.

The ultrathin SnO_2 based double ETL not only improves the PCE but also enhances the stability of the PSCs. Figure 5(a) shows the stabilized power output measurements of the PSCs with TiO_2 and TiO_2/SnO_2. The power output of the PSCs with double ETL exhibited negligible decay during the 1800 s measurement. However, the PCE of PSCs with only TiO_2 decreased quickly. The results suggest that the light stability of the PSCs is improved. Moreover, the light stability of the PSCs is further studied under continuous illumination. The PSCs with double ETL retained 85% of its initial PCE after 900 h continuous illumination without UV filter. On the contrary, the PCE of PSCs with TiO_2-only ETL quickly decayed to 64% of its initial value. The different light stability may arise from the photocatalysis properties of the TiO_2 ETL. The high chemical reactivity of TiO_2 under UV-light leads to the degradation of perovskite materials. Although the ultrathin SnO_2 layer only has a thickness around 5 nm, the compact and pinhole-free features effectively protect the perovskite film from photocatalysis degradation caused by TiO_2.

4. Conclusion and perspectives

In this work, we demonstrated an ultrathin SnO_2 layer based TiO_2/SnO_2 double ETL for efficient and stable PSCs. The ultrathin SnO_2 layer fabricated by ALD process with a thickness of several nanometer modified the physical and chemical properties of the ETL significantly. The good wettability of the double ETL enhanced the perovskite grain size and film quality through promoting crystals growth. With an optimized SnO_2 thickness of 5 nm, the double ETL improved PCE of PSCs from 18.02% to 21.13%. The double ETL with enhanced electrical conductivity and reduced pin-holes led to lower series resistance and higher shunt resistance in the PSCs. The double ETLs also showed improved band alignments between ETL and perovskite which promotes the PSCs performance. The defects density at the ETL/perovskite interface was passivated by the ultrathin SnO_2 layer, leading to a higher V_{OC} in the PSCs. Owing to the low chemical reactivity of SnO_2 under UV light, the PSCs with double ETL showed remarkable light stability, retaining 85% of its initial PCE after 900 h under continuous illumination. Our work demonstrates the potential of using the scalable ALD process to efficiently modify the ETL materials with ultrathin layers to achieve efficient and stable PSCs.

Acknowledgements

We would like to thank the Analytical & Testing Center of Northwestern Polytechnical University for SEM, XPS, UPS characterizations.

This work is supported by the National Key R&D Program of China (Grant No. 2019YFB1503201), the National Natural Science Foundation of China (Grant Nos. 52172238, 52102304, 51902264, and 51902177), the Natural Science Foundation of Shanxi Province, China (Grant No. 2020JM-093), Joint Research Funds of Department of Science & Technology of Shaanxi Province and Northwestern Polytechnical University (Grant No. 2020GXLH-Z-014), Science Technology and Innovation Commission of Shenzhen Municipality (Grant No. JCYJ20190807111605472), and the Fundamental Research Funds for the Central Universities, China (Grant Nos. 3102019JC0005 and G2021KY05103).

References

[1] Kojima A, Teshima K, Shirai Y and Miyasaka T 2009 *J. Am. Chem. Soc.* **131** 6050

[2] Zhou H, Chen Q, Li G, Luo S, Song T B, Duan H S, Hong Z, You J, Liu Y and Yang Y 2014 *Science* **345** 542

[3] Li C, Wang Z S, Zhu H L, Zhang D, Cheng J Q, Lin H, Ouyang D and Choy W C H 2018 *Adv. Energy Mater.* **8** 1801954

[4] Zhao D W, Chen C, Wang C L, Junda M M, Song Z N, Grice C R, Yu Y, Li C W, Subedi B, Podraza N J, Zhao X Z, Fang G J, Xiong R G, Zhu K and Yan Y F 2018 *Nat. Energy* **3** 1093

[5] Luo C, Zhao Y, Wang X, Gao F and Zhao Q 2021 *Adv. Mater.* **33** 2103231

[6] Xiao K, Lin R, Han Q, Hou Y, Qin Z, Nguyen H T, Wen J, Wei M, Yeddu V, Saidaminov M I, Gao Y, Luo X, Wang Y, Gao H, Zhang C, Xu J, Zhu J, Sargent E H and Tan H 2020 *Nat. Energy* **5** 870

[7] Zhu L, Zhang X, Li M, Shang X, Lei K, Zhang B, Chen C, Zheng S, Song H and Chen J 2021 *Adv. Energy Mater.* **11** 2100529

[8] Min H, Lee D Y, Kim J, Kim G, Lee K S, Kim J, Paik M J, Kim Y K, Kim K S, Kim M G, Shin T J and Il Seok S 2021 *Nature* **598** 444

[9] Bi D Q, Yi C Y, Luo J S, Decoppet J D, Zhang F, Zakeeruddin S M, Li X, Hagfeldt A and Gratzel M 2016 *Nat. Energy* **1** 16142

[10] Li S S, Chang C H, Wang Y C, Lin C W, Wang D Y, Lin J C, Chen C C, Sheu H S, Chia H C, Wu W R, Jeng U S, Liang C T, Sankar R, Chou F C and Chen C W 2016 *Energy Environ. Sci.* **9** 1282

[11] Liu Z, Qiu L, Juarez-Perez E J, Hawash Z, Kim T, Jiang Y, Wu Z, Raga S R, Ono L K, Liu S F and Qi Y 2018 *Nat. Commun.* **9** 3880

[12] Wu Y Z, Yang X D, Chen W, Yue Y F, Cai M L, Xie F X, Bi E B, Islam A and Han L Y 2016 *Nat. Energy* **1** 16148

[13] Zhao Y, Tan H, Yuan H, Yang Z, Fan J Z, Kim J, Voznyy O, Gong X, Quan L N, Tan C S, Hofkens J, Yu D, Zhao Q and Sargent E H 2018 *Nat. Commun.* **9** 1607

[14] Lee J W, Dai Z, Han T H, Choi C, Chang S Y, Lee S J, De Marco N, Zhao H, Sun P, Huang Y and Yang Y 2018 *Nat. Commun.* **9** 3021

[15] Liu T, Zhou Y, Li Z, Zhang L, Ju M G, Luo D, Yang Y, Yang M, Kim D H and Yang W 2018 *Adv. Energy Mater.* **8** 1800232

[16] Shao Y, Fang Y, Li T, Wang Q, Dong Q, Deng Y, Yuan Y, Wei H, Wang M and Gruverman A 2016 *Energy Environ. Sci.* **9** 1752

[17] Zong Y, Zhou Z, Chen M, Padture N P and Zhou Y 2018 *Adv. Energy Mater.* **8** 1800997

[18] Long C Y, Wang N, Huang K Q, Li H Y, Liu B and Yang J L 2020 *Chin. Phys. B* **29** 048801

[19] Abuhelaiqa M, Paek S, Lee Y, Cho K T, Heo S, Oveisi E, Huckaba A J, Kanda H, Kim H, Zhang Y, Humphry-Baker R, Kinge S, Asiri A M and Nazeeruddin M K 2019 *Energy Environ. Sci.* **12** 1910

[20] Arora N, Dar M I, Hinderhofer A, Pellet N, Schreiber F, Zakeeruddin S M and Gratzel M 2017 *Science* **358** 768

[21] Chen W, Xu L, Feng X, Jie J and He Z 2017 *Adv. Mater.* **29** 1603923

[22] Hou Y, Du X, Scheiner S, McMeekin D P, Wang Z, Li N, Killian M S, Chen H, Richter M, Levchuk I, Schrenker N, Spiecker E, Stubhan T, Luechinger N A, Hirsch A, Schmuki P, Steinruck H P, Fink R H, Halik M, Snaith H J and Brabec C J 2017 *Science* **358** 1192

[23] Kim Y C, Yang T Y, Jeon N J, Im J, Jang S, Shin T J, Shin H W, Kim S, Lee E, Kim S, Noh J H, Seok S I and Seo J 2017 *Energy Environ. Sci.* **10** 2109

[24] Li X, Yang J, Jiang Q, Lai H, Li S, Xin J, Chu W and Hou J 2018 *ACS Nano* **12** 5605

[25] Tu B, Shao Y, Chen W, Wu Y, Li X, He Y, Li J, Liu F, Zhang Z, Lin Y, Lan X, Xu L, Shi X, Ng A M C, Li H, Chung L W, Djurisic A B and He Z 2019 *Adv. Mater.* **31** 1805944

[26] Wojciechowski K, Leijtens T, Siprova S, Schlueter C, Horantner M T, Wang J T, Li C Z, Jen A K, Lee T L and Snaith H J 2015 *J. Phys. Chem. Lett.* **6** 2399

[27] Yang D, Yang R, Wang K, Wu C, Zhu X, Feng J, Ren X, Fang G, Priya S and Liu S F 2018 *Nat. Commun.* **9** 3239

[28] Gu Y F, Du H J, Li N N, Yang L and Zhou C Y 2019 *Chin. Phys. B* **28** 048802

[29] Hou S, Shi B, Wang P, Li Y, Zhang J, Chen P, Chen B, Hou F, Huang Q, Ding Y, Li Y, Zhang D, Xu S, Zhao Y and Zhang X 2020 *Chin. Phys. B* **29** 078801

[30] Burschka J, Pellet N, Moon S J, Humphry-Baker R, Gao P, Nazeeruddin M K and Gratzel M 2013 *Nature* **499** 316

[31] Giordano F, Abate A, Correa Baena J P, Saliba M, Matsui T, Im S H, Zakeeruddin S M, Nazeeruddin M K, Hagfeldt A and Graetzel M 2016 *Nat. Commun.* **7** 10379

[32] Ke W, Fang G, Wang J, Qin P, Tao H, Lei H, Liu Q, Dai X and Zhao X 2014 *ACS Appl. Mater. Interfaces* **6** 15959

[33] Li C, Li Y, Xing Y, Zhang Z, Zhang X, Li Z, Shi Y, Ma T, Ma R, Wang K and Wei J 2015 *ACS Appl. Mater. Interfaces* **7** 15117

[34] Lu H, Tian W, Gu B, Zhu Y and Li L 2017 *Small* **13** 1701535

[35] Jiang Q, Zhang X and You J 2018 *Small* **14** 1801154

[36] Kim J, Kim K S and Myung C W 2020 *npj Comput. Mater.* **6** 100

[37] Li Z, Wang Z, Jia C, Wan Z, Zhi C, Li C, Zhang M, Zhang C and Li Z 2022 *Nano Energy* **94** 106919

[38] Tavakoli M M, Yadav P, Tavakoli R and Kong J 2018 *Adv. Energy Mater.* **8** 1800794

[39] Xie H, Yin X, Liu J, Guo Y, Chen P, Que W, Wang G and Gao B 2019 *Appl. Surf. Sci.* **464** 700

[40] Valadez-Villalobos K, Idigoras J, Delgado L P, Meneses-Rodriguez D, Anta J A and Oskam G 2019 *J. Phys. Chem. Lett.* **10** 877

[41] Halvani Anaraki E, Kermanpur A, Mayer M T, Steier L, Ahmed T, Turren-Cruz S H, Seo J, Luo J, Zakeeruddin S M, Tress W R, Edvinsson T, Grätzel M, Hagfeldt A and Correa-Baena J P 2018 *ACS Energy Lett.* **3** 773

[42] Fang Z, Yang L, Jin Y, Liu K, Feng H, Deng B, Zheng L, Cui C, Tian C, Xie L, Xu X and Wei Z 2022 *Chin. Phys. B* **31** 118801

[43] Ren X, Yang D, Yang Z, Feng J, Zhu X, Niu J, Liu Y, Zhao W and Liu S F 2017 *ACS Appl. Mater. Interfaces* **9** 2421

[44] Shi X, Ding Y, Zhou S, Zhang B, Cai M, Yao J, Hu L, Wu J, Dai S and Nazeeruddin M K 2019 *Adv. Sci.* **6** 1901213

[45] Yang J, Xiong S, Song J, Wu H, Zeng Y, Lu L, Shen K, Hao T, Ma Z, Liu F, Duan C, Fahlman M and Bao Q 2020 *Adv. Energy Mater.* **10** 2000687

[46] Li C, Ma R, He X, Yang T, Zhou Z, Yang S, Liang Y, Sun X W, Wang J, Yan Y and Choy W C H 2020 *Adv. Energy Mater.* **10** 1903013